



Mechanical behaviors of single crystalline and fivefold twinned Ag nanowires under compression



S.B. Zhang

CAS Key Laboratory of Mechanical Behavior and Design of Materials, University of Science and Technology of China, Hefei, Anhui 230026, PR China

ARTICLE INFO

Article history:

Received 12 September 2014

Received in revised form 13 November 2014

Accepted 17 November 2014

Available online 6 December 2014

Keywords:

Fivefold twin

Compression

{001}⟨110⟩ Lomer dislocations

Cross-slip

ABSTRACT

The mechanical behaviors of fivefold twinned (FT) Ag nanowires under compression are investigated by molecular dynamics simulations. As a comparison, the single crystalline (SC) nanowires are also investigated. The fivefold twin boundary strengthens not only the tensile yield strength but also the compressive yield strength, suggesting the initial stress distribution is not the main factor behind the strengthening. The modulus-based explanation is also found invalid since similar modulus is observed between these two types of nanowires. In contrast to “dislocation starvation” state observed in SC nanowires under compression, the addition of fivefold twin boundary into nanowires leads to complex dislocation-dislocation and dislocation-twin interactions, contributing to increased dislocation density. While extend dislocation slip dominates the plastic deformation in SC nanowires, generation of {001}⟨110⟩ Lomer dislocations and their subsequent cross-slip are found to be the dominant deformation mechanisms in FT Ag nanowires under compression. Effects of boundary condition and sample geometry on plastic deformation behaviors are also investigated.

© 2014 Elsevier B.V. All rights reserved.

1. Introduction

In past decade, there has been a great deal of interest in exploring the plastic deformation characteristics of materials at the sub-micron scale. Uchic et al. [1] introduce a new approach to investigate the mechanical behavior of micron-scale single crystals (SC), fabricated by a focused ion beam (FIB), by uniaxial compression test in 2004. This technique opens up a era of mechanically test on various nanopillars [2–5]. The mechanical behavior of these nanopillars beyond the elastic regime is proved to be different from that of bulk materials. Experiments and Molecular dynamic (MD) simulations have demonstrated that yield in metal nanowires (NWs) is dictated by nucleation of Shockley partial dislocations from free surface [6–9]. Furthermore, since the confined volume, dislocations are likely to leave the small crystals before they have a chance to multiply, leading to “dislocation starvation” state. Plastic deformation thus requires nucleation of fresh dislocations from free surface at high stress, which results in the ubiquitously observed size effect of “the smaller, the stronger” and the emergence of intermittent discrete strain bursts [2,10].

Microstructure has a significant effect on the mechanical properties and mechanical behaviors of materials. Among which, the role of nanoscale twins on mechanical strength and plastic

deformation in nanomaterials has became a focus of research over last few years [11–25]. Ultrafine-grained copper containing layered growth nanotwins exhibits an unusual combination of ultrahigh yield strength and high ductility [11,12]. By modification of the twin boundary spacing, the mechanical properties can be further optimized [13,14]. The coherent twin boundaries can also significantly influence the limit of elasticity, ultimate strength, rate sensitively, activation volume, work hardening and fracture toughness of FCC metal NWs [15–22]. MD simulations are performed to obtain an atomically resolved observation of plastic deformation mechanisms to understand the role of twin boundary in real materials. The results show twin boundary not only acts as sources of dislocation nucleation [14,23] but also acts as obstacle for dislocations glide and slip transfer [14–16]. The dislocation-twin reactions are also investigated. The results show a dislocation with burgers vector of $1/2\langle110\rangle$ can nucleate and glide on a {100} plane instead of conventional {111} planes when a perfect dislocation transmits across twin boundary [24]. Recent study also shows the twin boundary can act as cleavage plane, resulting in ductile-to-brittle transition [25,26].

While a large number of studies have been conducted to investigate the mechanical behaviors of periodically twinned ⟨111⟩ NWs, knowledge about the role of fivefold twin boundary on mechanical behavior is still limited [27–33]. Notably, the technique of synthesizing FT NWs has been greatly improved [34,35].

E-mail address: zsbys@mail.ustc.edu.cn

Since the orientation of twin boundary with respect to loading axis is found to have significant effect on the mechanical behaviors [18], the deformation behaviors of FT NWs are expected to be quite different. Some novel deformation behaviors have been observed in FT NWs under tension. For example, Wu et al. [36] find the quinquefoliate flower pattern distribution of initial stress has a significant effect on subsequent mechanical behaviors of FT NWs. By combining experiments and MD simulations, Filleter et al. [37] find surface nucleation of stacking fault decahedrons (SFD) in multiple plastic zones distributed along the axis is the governing deformation mechanism in FT Ag NW under tension. Recently, Jiang et al. claims formation of quasi-icosahedral structures in necking region could also be a possible mode for plastic deformation in FT NWs under tension [38]. However most atomistic calculations have been performed considering axial tensile loading, while comparably few results exist for compression tests [32]. It is well known that the deformation behaviors of NWs under tension and compression are quite different. For example, the $\langle 110 \rangle$ Au NWs are found to deform by dislocation slip under compression and by twinning under tension [39]. The periodically twinned $\langle 111 \rangle$ NWs also display different deformation behaviors under tension and compression [40]. Therefore, it is of great interest to investigate the plasticity of FTNW under compression, which will greatly enrich our knowledge about the twin-mediated plasticity.

2. Simulation methods

Large-scale MD simulations of uniaxial compression tests are performed on $\langle 110 \rangle$ SC and FT Ag NWs using LAMMPS code [41] with time step of 2 fs. The interaction is described by the embed atom method (EAM) potential developed for Ag [42]. The cross-sectional geometries of models considered in this work are displayed in Fig. 1. Each model has diameter of about 20 nm and initial length of about 40 nm. Here the diameter is defined for the circumscribed circle of the pentagonal cross section. Two kind of boundary conditions, viz periodic boundary condition and free boundary condition [6–8,32], are applied along the axial direction respectively, while the other two directions are kept free.

Prior to loading, all samples are relaxed by conjugate gradient energy minimization followed by NVT relaxation for NWs with free boundary condition and by NPT relaxation for NWs with periodic boundary condition at 0.1 K for 20 ps to obtain equilibrated configurations. Compression is performed by imposing displacement to atoms along the long axial direction that varies linearly from zero at bottom to a maximum value at the top layer for NWs with free boundary condition [6,7] and by homogeneously re-scaling the coordinates of all atoms for NWs with periodic boundary condition [8,32]. Regardless of load methods, the samples are relaxed between each increment of strain for 20 ps in NVT ensemble at 0.1 K. The resulting strain is about $5.0 \times 10^7 \text{ s}^{-1}$. The atomic stress is computed by the virial scheme [43]. The local atomic shear strain [44] and central symmetry parameter (CSP) [45] are utilized to

analyze the defect structures. Images in this paper are created using OVITO package [46].

3. Results and discussion

3.1. Initial stress distribution

It is well known that surface tensile stress induces intrinsic compressive stress at the interior of metal NWs during relaxation, which has a significant effect on the yield behaviors of NWs [17,47]. Diao et al. [47] propose that the ubiquitously observed size effect on yield stress mainly results from the size dependent intrinsic compressive stress in metal NWs. Therefore, it is necessary to investigate the initial stress distribution in relaxed NWs. Fig. 2 shows the initial stress distribution over the cross-sections of SC and FT Ag NWs after NVT relaxation at 0.1 K (similar results are also found in the case of NPT relaxation). As can be seen from Fig. 2a3 and b3, the initial distribution of Von Mises stress and axial stress over the cross-section of SC Ag NW is quite uniform. Although it is widely recognized that fivefold twin boundary significantly alters the distribution of intrinsic stress, the detail of the distribution of intrinsic stress in FT NW is still controversial [48]. A recent study by Wu et al. [37] shows a quinquefoliate flower pattern distribution of stress in equilibrated FT Fe NWs, whereas similar distribution is barely observed in other metals, such as Cu [27], Pt [30], Ag [48]. Our current results show the quinquefoliate flower pattern distribution of Von Mises stress with a local maximum distributing in the shape of five leaflets running along the twin boundaries indeed exists in relaxed FT Ag NWs (see Fig. 2a2). Moreover, in addition to circular FT NW reported by Wu et al. [37], the pentagonal FT NW also displays analogous distribution (see Fig. 2a1). For completeness, we also investigate the effect of temperature on the initial distribution of stress in equilibrated FT NWs by performing relaxation at 300 K, analogous distribution of initial stress still can be observed. This result refutes the speculation by Sun et al. [48] that the reason why they have not observed the specific distribution of initial stress is because the different temperature used in their simulations. A possible reason behind these different observations may be the inappropriate image rendering method by some researchers. In order to distinguish the specific distribution, the stress range of color legend has to be carefully adjusted, therefore the precise magnitude of maximum stress and minimum stress cannot be read out directly from Fig. 2. Anyway, one still can find out the core of FT NW is highly compressed area and considerable tensile area exists in the vicinity of free surface (see Fig. 2b). Furthermore, the axial stress in the core is considerably higher in FT NW than in SC NW.

3.2. Mechanical properties

The typical compressive stress-strain curves of the three samples are shown in Fig. 3. Under loading, all samples first undergo

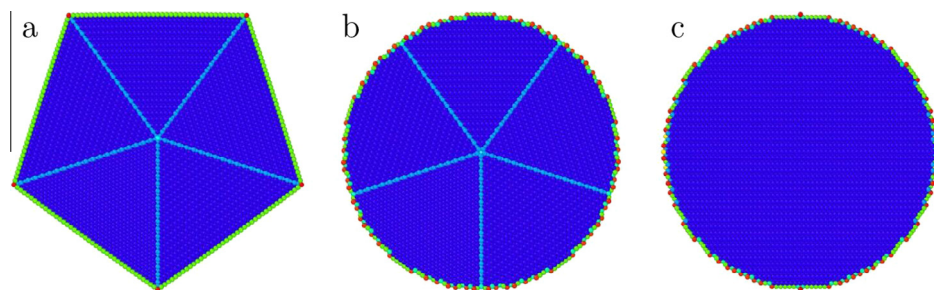


Fig. 1. The cross-sectional geometries and microstructures of models considered in this work. Atoms are colored according to CSP. (For interpretation of the references to color in this figure legend, the reader is referred to the web version of this article.)

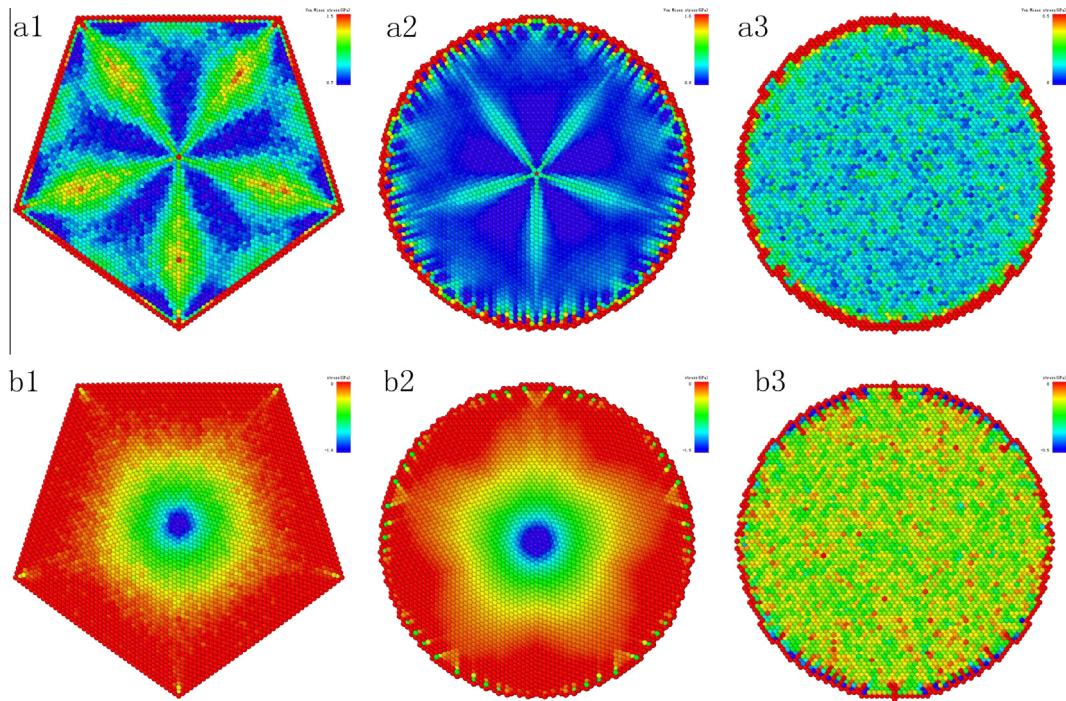


Fig. 2. Intrinsic stress distribution over the cross-section of equilibrate nanowires. Top: von Mises stress. Down: axial stress. The pentagonal FT NW, circular FT NW, and SC NW are arranged from left to right respectively. The stress range of color legend has been carefully adjusted. (For interpretation of the references to color in this figure legend, the reader is referred to the web version of this article.)

elastic deformation. Beyond a critical strain, the stress drops abruptly, which corresponds to emission of partial dislocation from free surface as evidenced by previous MD simulations [6–8,27–32]. The stress at this critical condition is called yield strength, and the critical strain is called yield strain. Young's modulus, yield strength, and yield strain are extracted from the stress–strain curves and listed in Table 1. Three main features can be summarized from Table 1. (i) The SC and FT NWs demonstrate similar Young's modulus of about 106 GPa regardless of boundary condition. (ii) Regardless of boundary condition, FT NWs show higher yield strength than SC NWs. For example, when considering the case of free boundary condition, the yield strength of FT NW with circular cross-section shape is 8.42 GPa, while the yield strength of SC NW is 6.67 GPa. There is an obvious strength increase, 1.75 GPa, a 26.28% increase of strength. (iii) Regardless of microstructure and geometry, the yield strength is pronounced higher in NWs with periodic boundary condition than in NWs with free boundary condition.

It is of great interest to compare the current results with available results. We begin our discussion with the Young's modulus. Past conclusions about the effect of twin boundary on Young's modulus are controversial. While some simulation results reveal stiffer elastic behavior of FT NWs when compared with twin-free NWs of the same size [28,29], most simulation results reveal similar Young's modulus between these two types of NWs [27,30–33,48,49]. All of these results are obtained from tensile

tests. Our current compressive simulation results clearly show the fivefold twin boundary has little effect on the Young's modulus. It needs to be mentioned that the magnitude of modulus measured in this work is consistent with published results from tensile MD simulations (100–113 GPa) [31,33,49] and is in the range of results measured in experiments (102 ± 23 GPa) [50]. The stiffness phenomenon observed by Yoo et al. [29] may arise from their test method. In their simulations, the NWs are strained in the range of 0–0.5% at increments of 0.1% along the axial direction. This process produces only six data points available for fitting the modulus. Since modulus is very sensitive to fitting process, their results may be inaccurate. Stiffness phenomenon is also mentioned by Leach et al. [28]. Unfortunately, they do not give the values of modulus in their paper. Notably, experimentally results tend to suggest similar Young's modulus between these two types of NWs [50].

Although past MD simulations reveal a higher tensile yield strength in FT NW than in SC NW [27,28,30–32,48], whether the fivefold twin boundary can strengthen the NWs under compression or not is still not clear. Leach et al. [28] attribute the higher yield strength to the increased elastic modulus. However, as mentioned above, similar modulus is observed between these two types of NWs, therefore the modulus is not the main factor behind the different yield strengths observed in this work. In addition, Leach et al. assume the yield strain is held constant, however, as can be seen in Table 1, the yield strain is also higher in FT NWs than in SC NWs. Sun et al. [32,48] attribute the higher yield strength to the higher initial compressive stress in the interior of FT NWs. Whereas their explanation inevitably predicts strengthening effects during tension and weakening effects during compression caused by five-fold twin boundary, which is contradictory to our results. A close observation of the initial stress distribution may suggest intrinsic compressive stress even fails at explaining the tensile MD simulation results. As shown in Fig. 2b, higher initial compressive stress indeed exists in the core of FT NW than in SC NW. However, yielding of NWs is controlled by nucleation of partial dislocations from free surface [47,51], it thus is a surface-dominated phenomenon. The

Table 1

Summary of the mechanical properties of NWs subjected to compressive load at 0.1 K. NWs with periodic boundary condition and free boundary condition along the axial direction are indicated by P and S respectively. FT NWs with circular and pentagonal cross-sections are indicated by FT1 and FT2 respectively.

Sample	Modulus (GPa)		Yield strain		Yield strength (GPa)	
	P	S	P	S	P	S
SC	105.5	107.3	−0.066	−0.043	11.343	6.668
FT1	106.4	106.6	−0.074	−0.051	13.920	8.421
FT2	104.6	106.5	−0.068	−0.048	11.916	7.601

stress at the vicinity of surface may play a dominant role. Obviously, atoms locate between surface and the starlike region are in tensile state in FT NWs (see Fig. 2b and Ref. [37]). Therefore the initial stress distribution is also not the main factor that contributes to the different yield strengths. The higher yield strength in FT NWs may arise from the image force from twin boundary. To nucleate a dislocation from free surface, a higher load must be applied to overcome the image force regardless of tension and compression. The image force model has successfully used to explain the ubiquitously observed size effect on yield strength in periodically twinned $\langle 111 \rangle$ NWs [17,21,52].

A higher yield strength observed in NWs with periodic boundary condition than in NWs with free boundary condition is not surprising. This is caused by different load methods used in both cases. For NWs with free boundary condition, a few layers of atoms at bottom and top are restricted, thence stress concentration inevitably exists on the interfaces between both ends and intermediate region [15]. The first partial dislocation prefers to nucleate from the stress concentration region and a lower yield strength is required. The difference in yield stress between pentagonal FT NW and circular FT NW can be understood from the different dislocation nucleation zones. In pentagonal FT NW, the first dislocation is nucleated at the intersection between free surface and twin boundary. In circular FT NW, the first dislocation is nucleated from free surface. The dislocation nucleation zone observed in this work is in line with previous results [27,36]. The different dislocation nucleation zones lead to different activation energy required for dislocation nucleation and contributes to different yield stress [8].

3.3. Plastic deformation mechanisms

3.3.1. SC NWs

The deformation mechanisms of SC NWs have been frequently investigated by MD simulations and experiments [39,51]. Here we simply describe the deformation process of SC NW under compression. Fig. 4a shows the atomic snapshots of SC NWs with free boundary condition under compression. Local shear strain and CSP are used to analysis the atomic snapshots. While CSP can identify defect structures, such as stacking fault and twin, the local shear strain can identify the accumulated plastic deformation. As can be seen in Fig. 4a, the plastic deformation in SC NW under compression is dominated by perfect dislocation slip, which is consistent with prediction from Schmid factor [51]. The slip lines and surface steps, as the results of escape of dislocation from free surface, are clearly visible (see Fig. 4a1). The perfect dislocation slip can be captured by comparing Fig. 4a2 and a3. While Fig. 4a3 records traces of slip in some places inside the NW, stacking fault ribbons is not always visible at corresponding positions in Fig. 4a2. The absence of frequent interactions between dislocations and the escape of dislocations from free surface are in line with the serrated stress-strain curve shown in Fig. 3b. The snapshots of NW with periodic boundary condition under compression show the same activated slip systems (Fig. 4b), the only divergence is dislocation slip in this case is more severe. The divergence can be explained as follow. For NW with periodic boundary condition, since no stress concentration region exists, regions along the axis are equivalent, dislocations prefer to nucleate from different regions along the axis simultaneously (see Fig. 4b1), which increases the chance of interaction. While for NW with free boundary condition, dislocations mainly nucleate from stress concentration regions, therefore they are likely to leave the NW rapidly before they have chance to interact.

3.3.2. FT NWs

Fig. 5 shows the atomic snapshots of pentagonal FT NW following different compressive strains. The most striking finding is glide

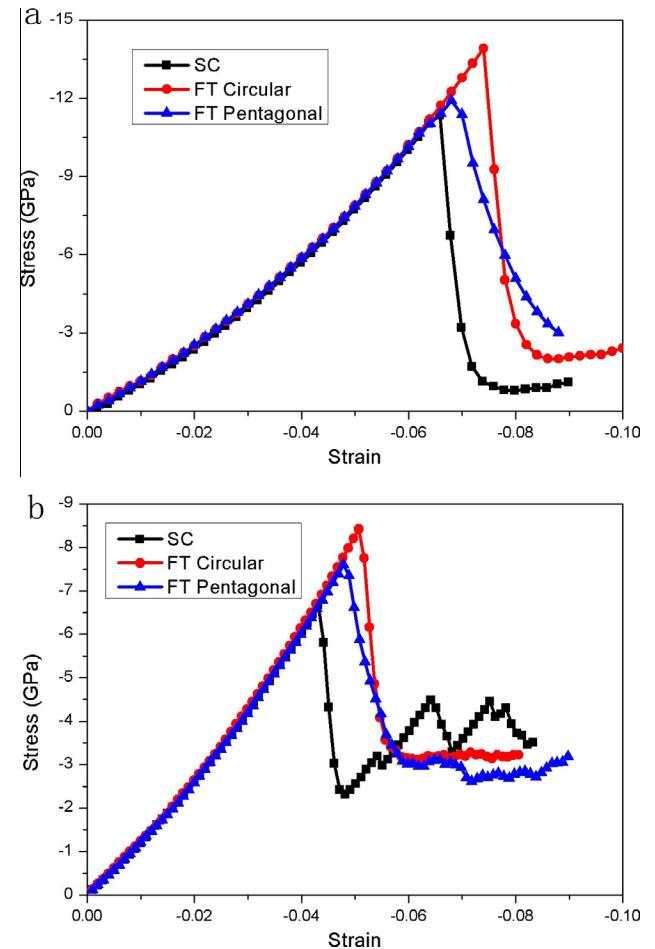


Fig. 3. Typical stress-strain curves of NWs with periodic (a) and free (b) boundary condition along the axial direction under compression at 0.1 K.

of dislocations on $\{100\}$ planes, instead of usual $\{111\}$ planes. Using the dislocation extraction algorithm (DXA) developed by Stukowski and Albe [54], we find these dislocations have burgers vector of $1/2\langle 110 \rangle$, viz $\{001\}\langle 110 \rangle$ Lomer dislocation. The generation of $\{001\}\langle 110 \rangle$ Lomer dislocation is observed in previous MD simulations on periodically twinned $\langle 111 \rangle$ NWs [15,16,19,24,53], and is believed to be a result of interaction of non-screw perfect dislocation with twin boundary [24]. This reaction can be expressed as

$$\frac{1}{2}\langle 011 \rangle \rightarrow \frac{1}{2}\langle \bar{1}0\bar{1} \rangle + \frac{1}{6}\langle \bar{1}\bar{1}2 \rangle \quad (1)$$

The novel deformation mechanism has not been observed in FT NW under tension because the trailing partial dislocation cannot be activated to catch up with the leading one to form perfect dislocation via combination of the two partials [33,36]. Two main factors can be responsible for the activation of trailing partial in FT NW under compression. First, Schmid factor suggests the extend dislocation slip is favorable under compression than under tension for $\langle 110 \rangle$ NW [51], this is confirmed by our simulation results on SC NW. Second, the leading partial is a 90° partial (pure edge) in FT NW under compression, while is a 30° partial under tension. Transmission of a 90° partial across twin boundary need to overcome a higher energy barrier, hence the 90° partial is most likely to be impeded at twin boundary, which gives chance to trailing partial to be activated.

The fivefold twin boundary also influences the activated slip systems. While only two of four $\{111\}$ slip planes are activated

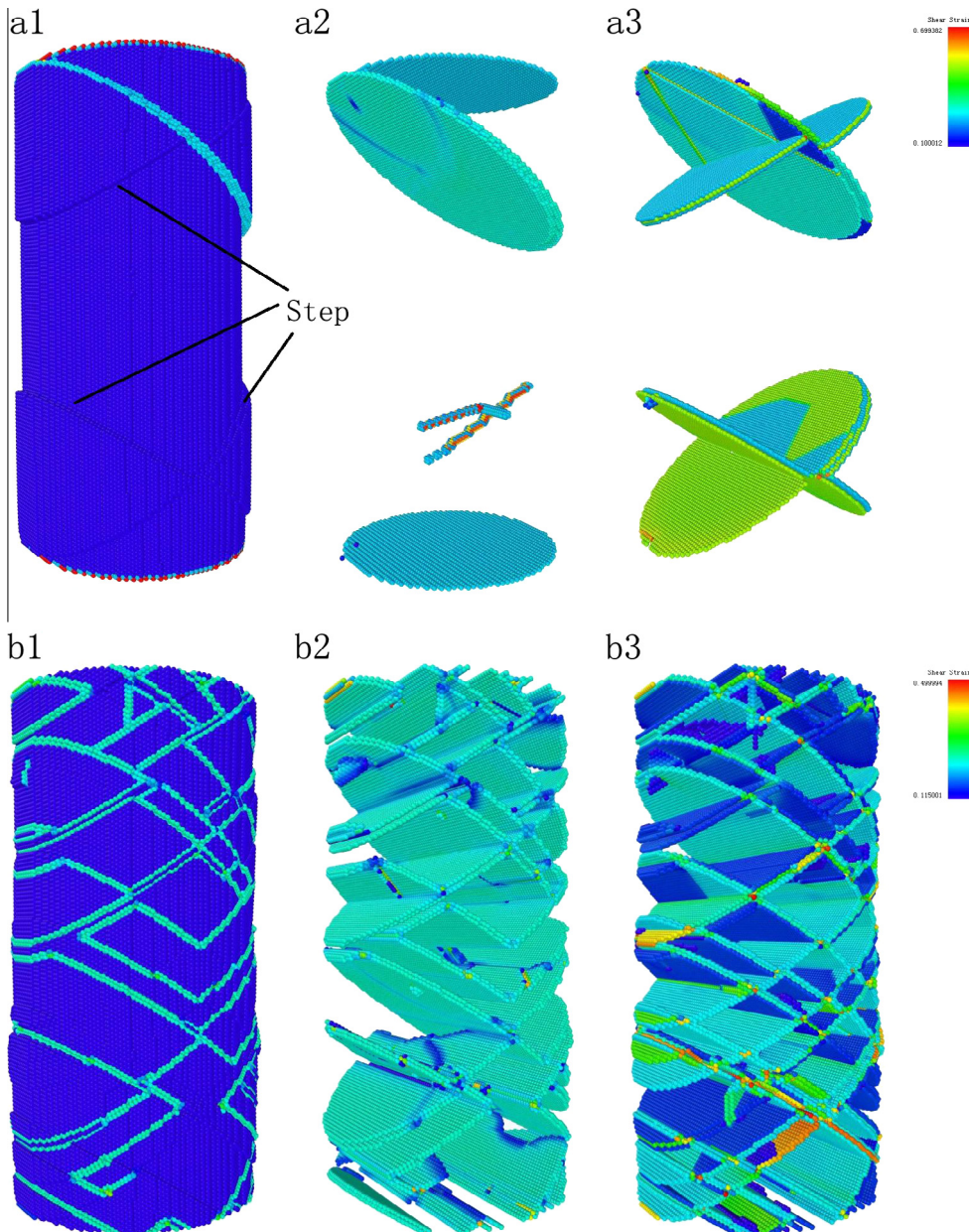


Fig. 4. Defect structures in SC NWs with free (a) and periodic (b) boundary condition during compressive deformation. All snapshots are recorded at the same strain of -0.083 . Atoms in a1–a2 and b1–b2 are colored according to CSP, perfect atoms in a2 and b2 are removed. Atoms in a3 and b3 are colored according to local shear strain, only atoms with shear strain in the range of $0.1\text{--}0.5$ are shown. (For interpretation of the references to color in this figure legend, the reader is referred to the web version of this article.)

in SC NWs, glide of dislocation on $\{111\}$ planes parallel to the load axis (with zero Schmid factor) has been observed in FT NW (see Fig. 5d–f). Previous MD simulations show glide of dislocation on $\{111\}$ twin planes perpendicular to axis in periodically twinned $\langle 111 \rangle$ NWs, causing detwinning or twin step [15,16,23,55]. This is caused by interaction of non-screw perfect dislocation with twin boundary [15,16]. In the present work, the observed dislocation slip on $\{111\}$ plane parallel to the axis is more likely to relate to cross-slip of anomalous $\{001\}\langle 110 \rangle$ Lomer dislocations. As can be seen from the atomic structure in Fig. 5d, as the Lomer dislocation loop expands, a section of the loop becomes parallel to the cross-line between the $\{100\}$ plane and the $\{111\}$ plane, hence is a screw segment, the screw segment then can easily cross-slip into $\{111\}$ plane. This cross-slip process is also expected to happen in nanotwinned polycrystalline metals and contributes to their ductility [53,55].

The whole process mentioned above can be illustrated by invoking the double Thomson tetrahedron. As shown in Fig. 6, the Thomson tetrahedron above and below the (111) twin plane ABC represents the matrix and the twin slip systems respectively. The loading direction is along AB. We extend the double Thomson tetrahedron by adding plane BMC and plane BMD*. BM is parallel to AD*, D*M is parallel to AB, therefore A, B, M, D* are on the same $\{111\}$ plane, both plane BCM and CMD* are $\{001\}$ plane. When a 60° perfect dislocation DB transmits across twin boundary ABC, it dissociates into a Shockley partial dislocation with burgers vector $C\bar{d}$ on plane ABC and a Lomer dislocation with burgers vector AD^* (or BM) on $\{001\}$ plane BMC, instead of usual $\{111\}$ plane ABD^* as described by Zhu et al. [56]. As the Lomer dislocation loop expanding on plane BMC, one end of the loop is truncated by free surface CMD^* and the other end is pinned at point B, eventually the loop becomes parallel to the cross-line BM between the $\{100\}$

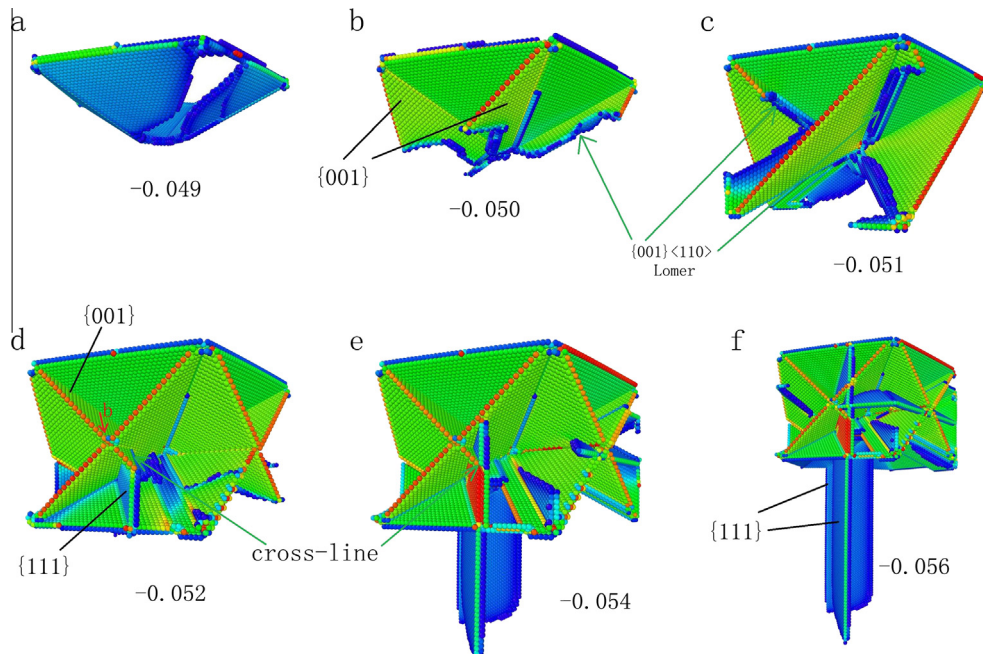


Fig. 5. Dislocation slip in pentagonal FT NW under compression. Atoms are colored according to local shear strain. The compressive strain are shown in each figure. Dislocations slip on anomalous {001} planes and {111} planes parallel to axis are observed. (For interpretation of the references to color in this figure legend, the reader is referred to the web version of this article.)

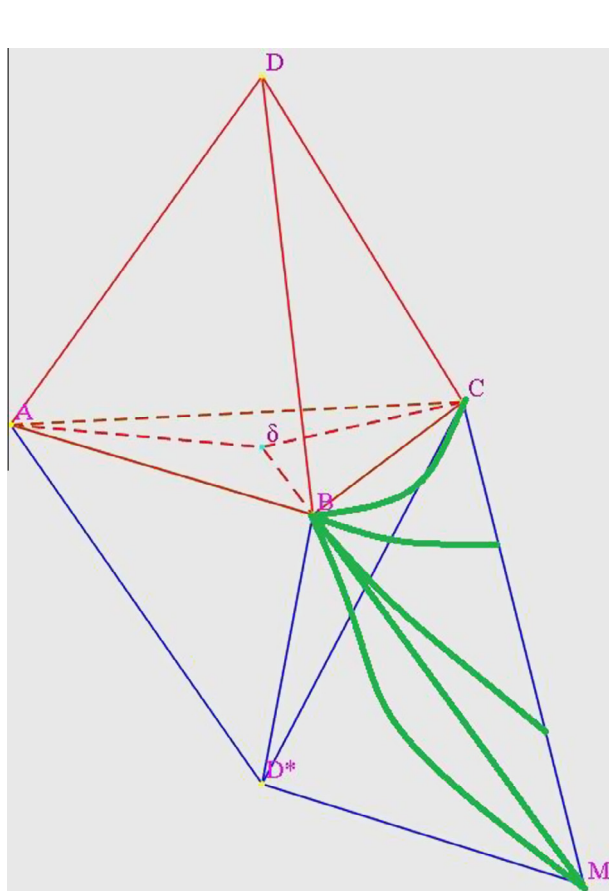


Fig. 6. Illustration of the deformation process by double Thompson tetrahedron. The tetrahedron above and below the twin plane ABC presents the matrix and the twin slip systems respectively. BM is parallel to AD*, D*M is parallel to AB, therefore A, B, M, D* on the same {1 1 1} plane, both BCM and CMD* are {001} plane. The olive thick solid lines show the expansion of dislocation loops.

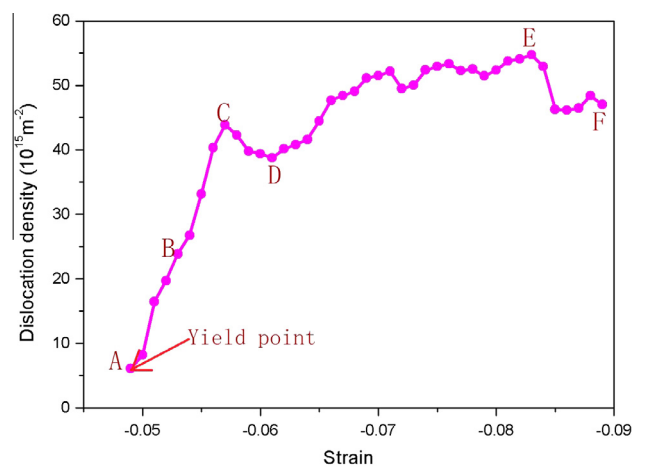


Fig. 7. Dislocation density as a function of applied strain in FT NW during compression.

plane BCM and the {111} plane ABMD* and is converted into a pure screw segment. The screw segment then can easily cross-slip into {111} plane ABMD*. A more complex process may be involved during the cross-slip process as proposed by Wu et al. [53,55]. For instance, the screw segment dissociates into a pair of Shockley partials on two different {111} planes and a stair-rod dislocation at the position of the original screw segment. However our present results show the Lomer dislocation dissociates into two Shockley partial dislocations on the same {111} plane ABMD*, which subsequently move towards both sides of the cross-line BM (see Fig. 5d, e).

In contrast to “dislocation starvation” state observed in SC NW (Fig. 4a2), the dislocation density in FT NW has been increasing. The evolution of dislocation density during deformation is plotted in Fig. 7. The dislocation density increases from $6.11 \times 10^{15} \text{ m}^{-2}$ at yield point to $5.48 \times 10^{16} \text{ m}^{-2}$ at strain -0.083 . The evolution of dislocation structures in FT NW under compression is displayed

in Fig. 8. The dislocation lines are extracted based on DXA [54], which is an efficient algorithm for identifying the dislocation length and burgers vector. This increased dislocation density should be attributed to the twin boundary which not only acts as

a barrier for dislocation propagation but also acts as dislocation multiplication source via interaction with dislocations [53,55]. Another important factor behind the increased dislocation density is the formation of dislocation junction (see Fig. 8). The dislocation

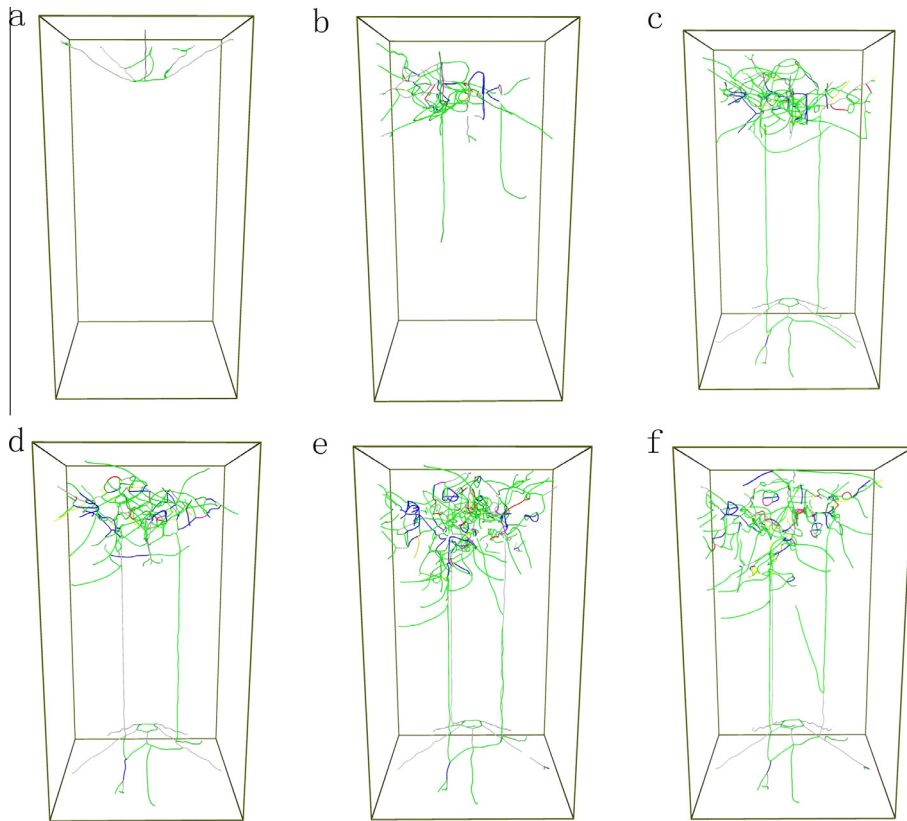


Fig. 8. Evolution of dislocation networks in FT NW during compression. Snapshots in a–f are related to the tagged points A–F in Fig. 7. The dislocations are extracted based on DXA. Green presents $1/6(112)$ Shockley partial dislocation, red presents $1/2(110)$ dislocation, magenta represents $1/3(110)$ type, blue represents $1/6(110)$ type, yellow represents $1/3(100)$ type. (For interpretation of the references to color in this figure legend, the reader is referred to the web version of this article.)

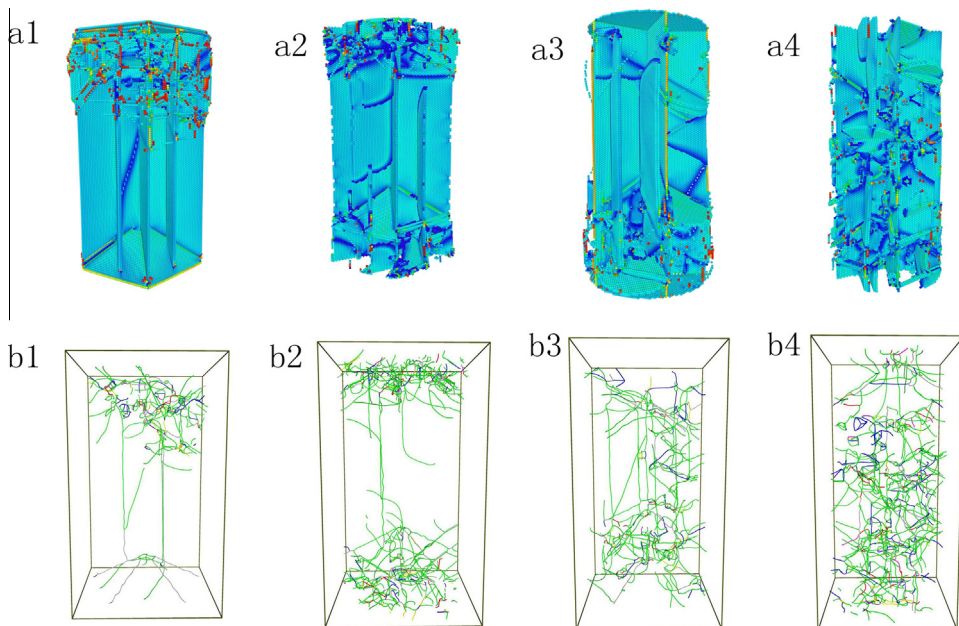


Fig. 9. Atomic structures (up) and dislocation structures (down) in NWs during compression. From left to right are pentagonal FT NW with free boundary condition, pentagonal FT NW with periodic boundary condition, circular FT NW with free boundary condition, circular FT NW with periodic boundary condition. Atomic are colored according to CSP in a, dislocation lines are colored according to dislocation types in b. (For interpretation of the references to color in this figure legend, the reader is referred to the web version of this article.)

junction is to a large extent caused by twin boundary which alters the orientations of slip planes. The intersection of dislocation lines with each other strongly limits their mobility. When two partial dislocations on different slip planes meet, they can form stair-rod dislocations. Four types of reactions have been proposed by Hirth and Lothe [57], of which, three are observed in the current simulations, viz

$$\frac{1}{6}\langle 2\bar{1}\bar{1} \rangle + \frac{1}{6}\langle \bar{1}2\bar{1} \rangle \rightarrow \frac{1}{6}\langle 110 \rangle \quad (2)$$

$$\frac{1}{6}\langle 1\bar{2}\bar{1} \rangle + \frac{1}{6}\langle 12\bar{1} \rangle \rightarrow \frac{1}{3}\langle 100 \rangle \quad (3)$$

$$\frac{1}{6}\langle \bar{1}12 \rangle + \frac{1}{6}\langle 112 \rangle \rightarrow \frac{1}{3}\langle 110 \rangle \quad (4)$$

Fig. 8 shows the stair-rod dislocations (colored magenta, blue and yellow) connecting stacking faults in two slip planes, where the magenta line segments correspond to $1/3\langle 110 \rangle$ type, blue line segments correspond to $1/6\langle 110 \rangle$ type, yellow line segments correspond to $1/3\langle 100 \rangle$ type. Generally, these stair-rod dislocations are sessile, thus provide obstacles to the motion of other glissile dislocations. Such high dislocation density and low mobility are the main factors behind the smooth stress-strain curve in **Fig. 3**.

We also investigate the effect of sample geometry and boundary condition on the deformation process of FT NW. **Fig. 9a** shows the atomic structures of all samples at the end of each simulation. The sample geometry and boundary condition do not alter the deformation mechanism. Lomer dislocation and cross-slip are observed in all samples. However the sample geometry and boundary condition indeed have considerable effect on the extent of dislocation slip. **Fig. 9b** shows the dislocation structures in FT NWs with different cross-section geometries and boundary conditions. In the case of free boundary condition, the dislocation density is $4.62 \times 10^{16} \text{ m}^{-2}$ in NW with pentagonal cross-section shape and is $8.12 \times 10^{16} \text{ m}^{-2}$ in NW with circular cross-section shape. In the case of periodic boundary condition, the dislocation density is $8.35 \times 10^{16} \text{ m}^{-2}$ in NW with pentagonal cross-section shape and is $1.56 \times 10^{17} \text{ m}^{-2}$ in NW with circular cross-section shape. The dislocation slip is more severe in NW with circular cross-section than in NW with pentagonal cross-section and is more severe in NW with periodic boundary condition than in NW with free boundary condition.

4. Conclusions

MD simulations are performed to investigate the compressive mechanical behaviors of SC and FT NWs. The initial stress distribution, the mechanical properties and the deformation mechanisms are carefully analyzed. The main results include:

- (1) The initial distribution of Von Mises stress in relaxed FT Ag NWs displays a quinquefoliate flower pattern with a local maximum distributing in the shape of five leaflets running along the twin boundaries. The core of FT NW is highly compressed area and considerable tensile area exists at the vicinity of surface.
- (2) Fivefold twin boundary strengthens not only tensile yield strength but also compressive yield strength of Ag NWs. The strengthening effects may arise from the image force from twin boundary which suppresses dislocation emission.
- (3) Generation of $\{001\}\langle 110 \rangle$ Lomer dislocations and their subsequent cross-slip are the dominant deformation mechanisms in FT Ag nanowires under compression.

- (4) While “dislocation starvation” state is observed in SC NWs under compression, the addition of fivefold twin boundary into NWs leads to complex dislocation-twin and dislocation-dislocation interactions, contributing to increased dislocation density.
- (5) Boundary condition and sample geometry do not alter the deformation mechanism, but influence the extent of dislocation slip.

References

- [1] M.D. Uchic, D.M. Dimiduk, J.N. Florando, W.D. Nix, *Science* 305 (2004) 986.
- [2] J.R. Greer, W.C. Oliver, W.D. Nix, *Acta Mater.* 53 (2005) 1821.
- [3] D.M. Dimiduk, M.D. Uchic, T.A. Parthasarathy, *Acta Mater.* 53 (2005) 4065.
- [4] D. Kiener, A.M. Minor, *Acta Mater.* 59 (2011) 1328.
- [5] A.T. Jennings, M.J. Burek, J.R. Greer, *Phys. Rev. Lett.* 104 (2010) 135503.
- [6] S. Xu, Y.F. Guo, A.H.W. Ngan, *Int. J. Plast.* 43 (2013) 116.
- [7] L.A. Zepeda-Ruiz, B. Sadigh, J. Biener, A.M. Hodge, A.V. Hamza, *Appl. Phys. Lett.* 91 (2007) 101907.
- [8] C.R. Weinberger, A.T. Jennings, K. Kang, J.R. Greer, *J. Mech. Phys. Solids* 60 (2012) 84.
- [9] H. Zheng, A.J. Cao, C.R. Weinberger, J.Y. Huang, K. Du, J. Wang, Y. Ma, Y. Xia, S.X. Mao, *Nat. Commun.* 1 (2010) 144.
- [10] S.H. Oh, M. Legros, D. Kiener, G. Dehm, *Nat. Mater.* 8 (2009) 95.
- [11] L. Lu, Y.F. Shen, X.H. Chen, L.H. Qian, K. Lu, *Science* 304 (2004) 422.
- [12] L. Lu, X. Chen, X. Huang, K. Lu, *Science* 323 (2009) 607.
- [13] L.L. Zhu, H.H. Ruan, X.Y. Li, M. Dao, H.J. Gao, J. Lu, *Acta Mater.* 59 (2011) 5544.
- [14] X.Y. Li, Y.J. Wei, L. Lu, K. Lu, H.J. Gao, *Nature* 464 (2010) 877.
- [15] K.A. Afanasyev, F. Sansoz, *Nano Lett.* 7 (2007) 2056.
- [16] C. Deng, F. Sansoz, *Nano Lett.* 9 (2009) 1517.
- [17] C. Deng, F. Sansoz, *Appl. Phys. Lett.* 95 (2009) 091914.
- [18] Z.S. You, X.X. Li, L.G. Gui, Q.H. Lu, T. Zhu, H.J. Gao, L. Lu, *Acta Mater.* 61 (2013) 217.
- [19] C. Deng, F. Sansoz, *Acta Mater.* 57 (2009) 6090.
- [20] C. Deng, F. Sansoz, *Phys. Rev. B* 81 (2010) 155430.
- [21] C. Deng, F. Sansoz, *ACS Nano* 3 (2009) 3001.
- [22] M. Dao, L. Lu, R.J. Asaro, J. Hosson, E. Ma, *Acta Mater.* 55 (2007) 4041.
- [23] J.J. Zhang, F.D. Xu, Y.D. Yan, T. Sun, *Chin. Sci. Bull.* 58 (2013) 684.
- [24] J. Wang, H.C. Huang, *Appl. Phys. Lett.* 88 (2006) 203112.
- [25] D.C. Jang, X.Y. Li, H.J. Gao, J. Greer, *Nat. Nanotechnol.* 7 (2012) 594.
- [26] J.W. Wang, F. Sansoz, J.Y. Huang, Y. Liu, S. Sun, Z. Zhang, S.X. Mao, *Nat. Commun.* 4 (2013) 1742.
- [27] A.J. Cao, Y.G. Wei, *Phys. Rev. B* 74 (2006) 214108.
- [28] A.M. Leach, M. McDowell, K. Gall, *Adv. Funct. Mater.* 17 (2007) 43.
- [29] J.H. Yoo, S. Oh, M.S. Jeong, J. Appl. Phys. 107 (2010) 094316.
- [30] Y.H. Wen, R. Huang, Z.Z. Zhu, Q. Wang, *Comput. Mater. Sci.* 55 (2012) 205.
- [31] Y.J. Gao, Y.Q. Fu, W. Sun, Y. Sun, H. Wang, F. Wang, J. Zhao, *Comput. Mater. Sci.* 55 (2012) 322.
- [32] M.F. Sun, R.G. Cao, F. Xiao, C. Deng, *Scripta Mater.* 69 (2013) 227.
- [33] S.B. Zhang, *Comput. Mater. Sci.* 95 (2014) 53.
- [34] J.J. Ma, M.S. Zhan, *RSC Adv.* 4 (2014) 21060.
- [35] H.J. Yang, S.Y. He, H.Y. Tuan, *Langmuir* 30 (2014) 602.
- [36] T. Filletter, S. Ryu, K. Kang, J. Yin, R.A. Bernal, K. Sohn, S. Li, J.X. Huang, W. Cai, D. Espinosa, *Small* 8 (2012) 2986.
- [37] J.Y. Wu, S. Nagao, J.Y. He, Z.L. Zhang, *Nano Lett.* 11 (2011) 5264.
- [38] S. Jiang, Y.G. Shen, Y.G. Zheng, Z. Chen, *Appl. Phys. Lett.* 103 (2014) 041909.
- [39] S. Lee, J. Im, Y.H. Yoo, E. Bitzek, D. Kiener, G. Richter, B. Kim, S.H. Oh, *Nat. Commun.* 5 (2014) 3033.
- [40] Y.F. Zhang, H.C. Huang, S.N. Atluri, *CMES* 35 (2008) 215.
- [41] S.J. Plimpton, *J. Comput. Phys.* 117 (1995) 1.
- [42] S.M. Foiles, M.I. Baskes, M.S. Daw, *Phys. Rev. B* 33 (1986) 7983.
- [43] M. Zhou, *Proc. R. Soc. Lond., Ser. A* 459 (2003) 2347.
- [44] F. Shimizu, S. Ogata, J. Li, *Mater. Trans.* 48 (2007) 2923.
- [45] C.L. Kelchner, S.J. Plimpton, J.C. Hamilton, *Phys. Rev. B* 58 (1998) 11085.
- [46] A. Stukowski, *Modell. Simul. Sci. Eng.* 18 (2010) 015012.
- [47] J.K. Diao, K. Gall, M.L. Dunn, J.A. Zimmerman, *Acta Mater.* 54 (2006) 643.
- [48] M.F. Sun, R.G. Cao, F. Xiao, C. Deng, *Comput. Mater. Sci.* 79 (2013) 289.
- [49] M.T. McDowell, A.M. Leach, K. Gall, *Nano Lett.* 8 (2008) 3613.
- [50] B. Wu, A. Heidelberg, J.J. Boland, *Nano Lett.* 6 (2006) 468.
- [51] C.R. Weinberger, Wei Cai, *J. Mater. Chem.* 22 (2012) 3277.
- [52] C. Deng, F. Sansoz, *Scr. Mater.* 63 (2010) 50.
- [53] Z.X. Wu, Y.W. Zhang, D.J. Srolovitz, *Acta Mater.* 57 (2009) 4508.
- [54] A. Stukowski, K. Albe, *Modell. Simul. Sci. Eng.* 18 (2010) 085001.
- [55] Z.X. Wu, Y.W. Zhang, D.J. Srolovitz, *Acta Mater.* 59 (2011) 6890.
- [56] Y.T. Zhu, X.L. Wu, X.Z. Liao, J. Narayan, L.J. Kecskes, S.N. Mathaudhu, *Acta Mater.* 59 (2011) 812.
- [57] J.P. Hirth, J. Lothe, *Theory of Dislocations*, Krieger Publishing Company, 1982.

Update

Computational Materials Science

Volume 101, Issue , 15 April 2015, Page 321

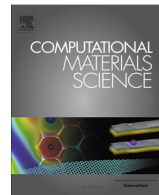
DOI: <https://doi.org/10.1016/j.commatsci.2015.02.012>



Contents lists available at ScienceDirect

Computational Materials Science

journal homepage: www.elsevier.com/locate/commatsci



Corrigendum

Corrigendum to “Mechanical behaviors of single crystalline and fivefold twinned Ag nanowires under compression” [Comput. Mater. Sci. 98 (2015) 320–327]



S.B. Zhang

CAS Key Laboratory of Mechanical Behavior and Design of Materials, University of Science and Technology of China, Hefei, Anhui 230026, PR China

The author informs that there are some errors in the published article.

The following corrections apply to Ref. [38]:

S. Jiang, Y.G. Shen, Y.G. Zheng, Z. Chen, Appl. Phys. Lett. 103 (2013) 041909.

DOI of original article: <http://dx.doi.org/10.1016/j.commatsci.2014.11.032>
E-mail address: zsbys@ustc.edu.cn